Applied Catalysis B: Environmental 256 (2019) 117864

Contents lists available at ScienceDirect

Applied Catalysis B: Environmental

journal homepage: www.elsevier.com/locate/apcatb

Dual function of graphene oxide for assisted exfoliation of black phosphorus and electron shuttle in promoting visible and near-infrared photocatalytic H_2 evolution

Mingshan Zhu[a], Mamoru Fujitsuka[b], Lixi Zeng[a,*], Minghua Liu[c], Tetsuro Majima[b,*]

[a] School of Environment, Jinan University, Guangzhou, 510632, PR China
[b] The Institute of Scientific and Industrial Research (SANKEN), Osaka University, Mihogaoka 8-1, Ibaraki, Osaka, 567-0047, Japan
[c] Beijing National Laboratory for Molecular Science, CAS Key Laboratory of Colloid, Interface and Chemical Thermodynamics, Institute of Chemistry, Chinese Academy of Sciences, Beijing, 100190, PR China

ARTICLE INFO

Keywords:
Black phosphorous
Graphene oxide
Hydrogen evolution
Visible and NIR
Noble-metal-free

ABSTRACT

The search for suitable photocatalysts with broadband absorption in visible and near-infrared (NIR) region is recognized as one of the most challenging issues on solar energy utilization. Black phosphorous (BP) is demonstrated as an effective visible and NIR activated material in solar energy conversion. However, traditional liquid exfoliation yield is low and the rigid structure and insoluble properties of pristine BP hinder its high-yield of hybridization. Herein, a new and stable noble-metal-free ternary photocatalyst molybdenum disulfide (MoS_2)-BP/graphene oxide (GO) was constructed for splitting water to H_2, showing dual functions of GO in synthetic and photocatalytic processes. Under visible-NIR light irradiation, the H_2 evolution rates of MoS_2-BP/GO was enhanced to 3.47 μmol h^{-1}. Rapid electron injection efficiency from excited BP to GO and to MoS_2 was confirmed by femtosecond transient absorption spectroscopy. This study provides new insight into the design of nanomaterials, and offers a noble-metal-free protocol with photocatalytic H_2 production.

1. Introduction

In regard to the high efficiency of light–chemical energy conversion, the search for suitable photocatalysts with full spectrum solar light absorption from UV to near-infrared (NIR) region is one of the most challenging missions. Two dimensional (2D) materials, owing to their unique properties and widespread applications, received a great deal of interest on both fundamental researches and practical applications [1–4]. Beside star material of graphene, more and more atomic thickness 2D and quasi-2D materials were developed in the past decade [2–4]. As a member in group V of the periodic table, phosphorus (P) accounts for approximately 0.1% of the earth's crust and the black phosphorus (BP) is the most thermodynamically stable at room temperature and nontoxic among P allotropes [5]. Similar to graphite, BP has a layered structure to consist of a single element of P (Scheme 1a) and it can be liquid to be exfoliated into single-/few-layers structures. Very recently, BP nanosheets grab a great attention since the successful first report of atomic layer thick BP on field-effect transistor in 2014 [6–10]. Different from graphene, BP has a bandgap in the ranges from 0.3 eV (in bulk form) to 2.1 eV (in monolayer form), indicating that BP can act as an effective photo-activated material in optical device and solar energy conversion under visible and near-infrared (NIR) irradiation [11–28]. For example, we successfully used 2D BP nanosheets as effective visible and NIR-driven photocatalysts for the application of water splitting to H_2 [19–24].

In general, BP nanosheets were prepared by liquid exfoliation in organic solvent such as *N*-methyl-2-pyrrolidone (NMP) [29]. However, it needs long sonication time and the exfoliation yield is low. Moreover, to obtain high quantum efficiency on photocatalytic H_2 production, a co-catalyst is needed to hybrid with BP owing to the fast recombination of photogenerated electron-hole pairs in pure BP. The rigid structure and insoluble properties of pristine BP hinder its high-yield of hybridization. To address this tough challenge, discovering a new protocol of exfoliated BP nanosheets is necessary.

Recently, high-quality nanosheets of 2D materials including graphene, molybdenum disulfide (MoS_2), cobalt hydroxide [$Co(OH)_2$], etc. were achieved by using liquid exfoliation with the assistance of graphene oxide (GO) [30–32]. GO, a 2D structure whose basal plane and edge are decorated with abundant oxygen containing functional groups (carboxyl, hydroxyl, epoxide, etc., Scheme 1b), has been verified to be a

* Corresponding authors.
E-mail addresses: lxzeng@jnu.edu.cn (L. Zeng), majima@sanken.osaka-u.ac.jp (T. Majima).

https://doi.org/10.1016/j.apcatb.2019.117864
Received 6 May 2019; Received in revised form 8 June 2019; Accepted 12 June 2019
Available online 12 June 2019

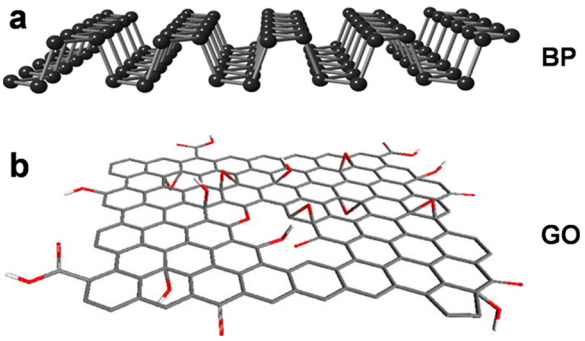

Scheme 1. Schematic structures of single layer BP (a) and GO sheet (b).

2D surfactant [33,34]. The presence of GO prevents the restacking of nanosheet structures during exfoliation from precursors [32]. Moreover, owing to its locally conjugated aromatic system and basal plane and edge with decorated diverse oxygen containing functional groups, GO is verified to be an excellent catalyst carrier and promoter [34]. In view of the foregoing, as shown in Scheme 2, we used GO to assist the exfoliation of bulk BP. Afterwards, noble-metal-alternative co-catalyst of MoS_2 was introduced to prepare the ternary composite of MoS_2-BP/GO for the application of water reduction to H_2. Compare to BP/GO and MoS_2-BP, 13.3 and 2.27 folds were obtained in the ternary composite of MoS_2-BP/GO for photocatalytic H_2 production under visible and NIR light irradiation, respectively. Herein, GO shows dual functions in both synthetic and photocatalytic processes. Firstly, GO acts as a surfactant to assist the exfoliation of bulk BP. Because of the abundant functional groups of GO, (i) the as-prepared BP/GO has well-dispersibility in NMP solvent for a long time (Fig. S1); (ii) the GO acted as a coupling reagent, i.e., the additive co-catalyst of MoS_2 can be well decorated on the surface of BP/GO. These two advantages are both in favor of the photocatalytic reaction. Secondly, owing to its locally conjugated aromatic system and nice electron shuttle ability, the GO promotes an efficient charge separation/transfer during photocatalytic reaction, resulting in the enhanced photocatalytic performance.

2. Experimental section

2.1. Materials

Bulk BP (XF161), single layer of GO (XF002-1), and bulk MoS_2 crystals (XF184-1) were purchased from Nanjing XFNANO Materials Tech Co., Ltd. N-methyl-2-pyrrolidone (NMP), methanol, and all other chemical materials were purchased from Sigma-Aldrich, and used without further purification.

2.2. Preparation of BP/GO

BP/GO was obtained through a NMP solvent exfoliation method in the presence of GO. The bulk BP crystals (XF161, purity > 99.998%) and single layer of GO (XF002-1, purity~99%) were purchased from Nanjing XFNANO Materials Tech. Firstly, 10 mg single layer GO was dispersed into 100 mL NMP solvent with sonication for 2 h, resulting GO/NMP dispersion (0.1 mg mL^{-1}). Secondly, 20 mg bulk BP was added into above 20 mL GO/NMP. The dispersion was then sonicated for 3 h with a tip sonicator (Misonix XL-2000) at 10 W output power and ice cooling. After exfoliation, the dispersion was centrifuged at 4000 rpm for 20 min with two times to remove bulk BP, resulting in BP/GO NMP dispersion (0.4 mg mL^{-1}). Pure 2D BP nanosheets were obtained by similar method in the absence of GO.

2.3. Preparation of MoS_2-BP/GO

MoS_2-BP/GO was prepared as follows: 20 mL as-prepared MoS_2 NMP dispersion was added into 50 mL BP/GO NMP dispersion with sonication for 2 h. The mixtures were kept stirring overnight. Finally, the samples were obtained through high-speed centrifugation and washed with ethanol thoroughly, and then re-dispersed in 5.5 mL methanol, resulting in MoS_2-BP/GO (0.4 mg mL^{-1}). The weight ratio of MoS_2 to BP/GO was 1:10. Before reaction, the MoS_2-BP/GO dispersion was collected by high-speed centrifugation and re-dispersed in aqueous solution.

2.4. Photocatalytic H_2 production

1 mL MoS_2-BP/GO aqueous dispersion (0.4 mg mL^{-1}) and 1 mL methanol mixed with 3 mL water were added into a 35 mL cylinder reactor and sealed with a rubber septum. The sample was deaerated by Ar bubbling into the solution for 30 min before the reaction. The solution was stirred continuously and irradiated by a Xenon lamp (Asahi Spectra, HAL-320W, output wavelength of 350~1800 nm) with a 420-nm long pass filter at room temperature. The gases produced were analyzed with a gas chromatograph (Shimadzu GC-8A) equipped with an MS-5A column and a thermal conductivity detector (TCD).

2.5. Transient absorption measurements

The transient absorption spectra were measured by the pump and probe method using a regeneratively amplified titanium sapphire laser (Spectra-Physics, Spitfire Pro F, 1 kHz) pumped by a Nd:YLF laser (Spectra-Physics, Empower 15). The seed pulse was generated by a titanium sapphire laser (Spectra-Physics, Mai Tai VFSJW; fwhm 80 fs). The second harmonic generation of the fundamental light (400 nm, 3 μJ $pulse^{-1}$) was used as the excitation pulse. A white light continuum pulse, which was generated by focusing the residual of the fundamental light on a sapphire crystal after the computer controlled optical delay, was divided into two parts and used as the probe and the reference lights, of which the latter was used to compensate the laser fluctuation. The samples were sealed in a cuvette with rotating that the absorptions of the NMP dispersion at 400 nm were adjusted to ~1.0 OD by using 2 mm path length of quartz cuvette. The pump pulse was chopped by

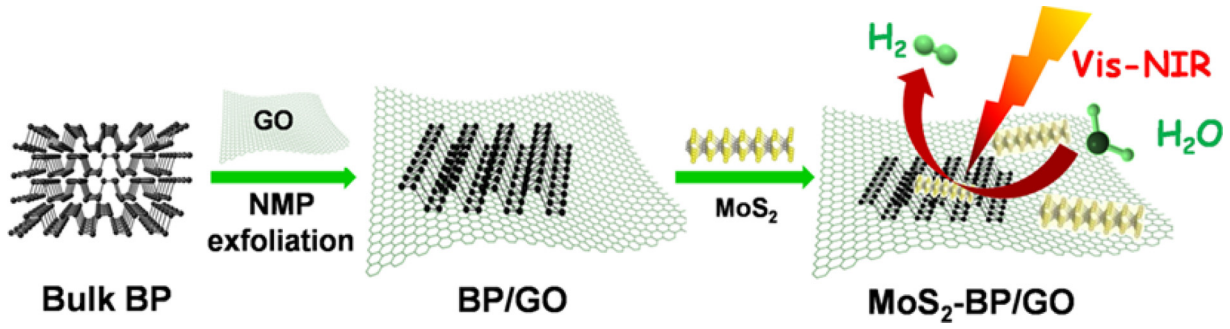

Scheme 2. Scheme of synthetic process of MoS_2-BP/GO for H_2 evolution.

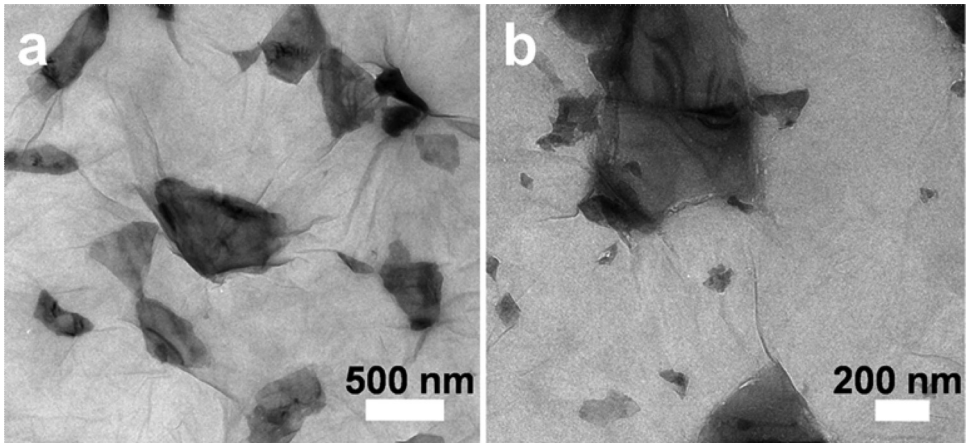

Fig. 1. TEM images of as-prepared BP/GO (a) and MoS_2-BP/GO (b).

the mechanical chopper synchronized to one-half of the laser repetition rate, resulting in a pair of spectra with and without the pump, from which the absorption change induced by the pump pulse was estimated. All measurements were carried out at room temperature.

3. Results and discussion

As shown in Scheme 2, BP nanosheets were easily obtained by using liquid-phase exfoliation of bulk BP with assistance of GO. Fig. 1a clearly shows the as-prepared of BP/GO nanosheets in which the 2D BP nanosheets were well assembled on the surface of GO nanosheets after exfoliation for 3 h. The size of the as-prepared BP nanosheets on the surface of GO nanosheets is approximately 300 nm to 1.0 μm. The different components of BP and GO were further confirmed by HAADF-STEM and energy-dispersive X-ray spectroscopy (EDS) elemental mappings and spectrum (Figs. 2 and S2). In the STEM image, some pieces of bright nanosheets were easily observed on the silk-like structures. On the other hand, in the images of EDS elemental mappings, the elemental phosphorus extracted from the spectrum image confirms that the phosphorus signal is strongly correlated with the bright nanosheets locations. Besides, all elements of C, O, and P are detected in the as-prepared samples in the spectrum of EDS. The crystallinity of the as-prepared BP was further investigated by high-resolution TEM (HRTEM) (Fig. S3), in which clear lattice fringes with d-spacing of 0.22 nm were detected to be matched with (002) planes of BP nanosheets [11,21].

In the photocatalytic H_2 evolution, a noble metal such as platinum (Pt) is generally used as extra co-catalyst for improving the efficiency of H_2 production. However, the high-cost of Pt forces us to explore various noble-metal-alternative co-catalysts [23,35]. Currently, 2D-layered transition metal disulfides (TMDs) such as MoS_2 nanosheets have been regarded as promising noble-metal-free co-catalyst for H_2 production owing to its intrinsic electronic property [35]. Hence, 2D MoS_2 nanosheets were introduced to improve the efficiency of photocatalytic H_2 production for BP/GO. MoS_2 nanosheets were obtained by liquid

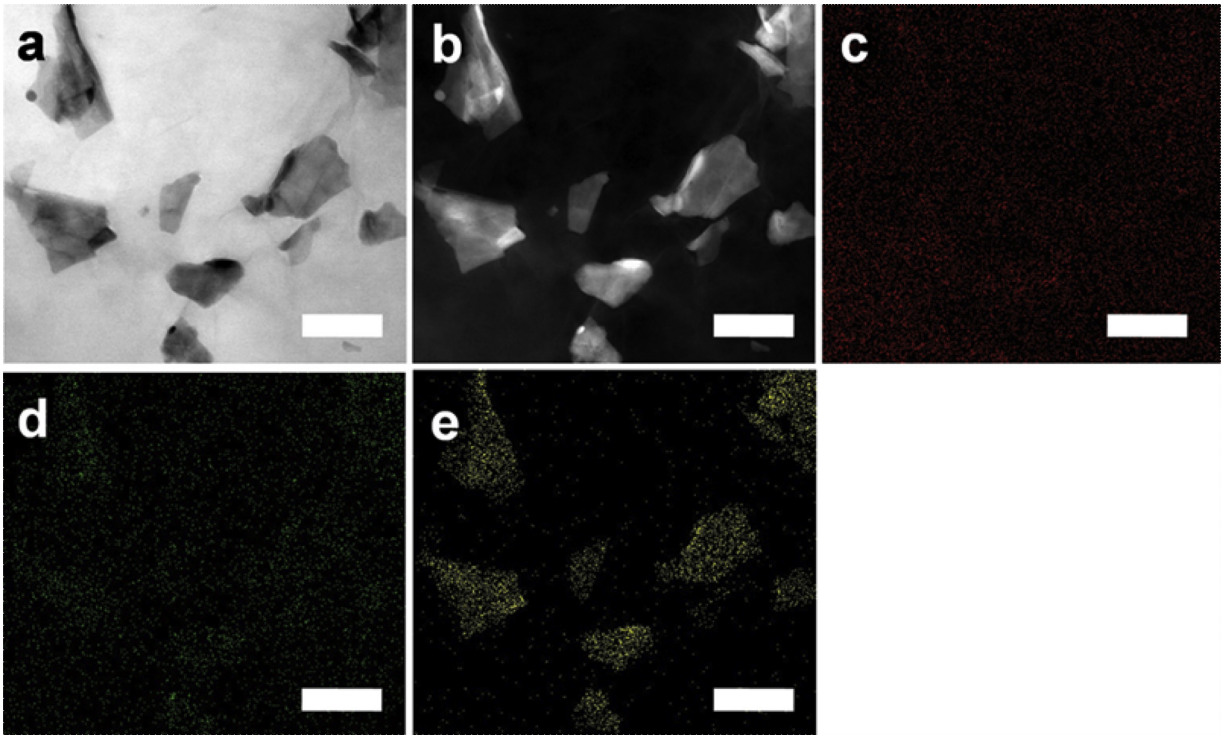

Fig. 2. TEM (a) and HAADF-STEM (b) images of BP/GO and corresponding EDS elemental mapping of C (c), O (d), and P (e) elements. The scale bars are 500 nm in the images.

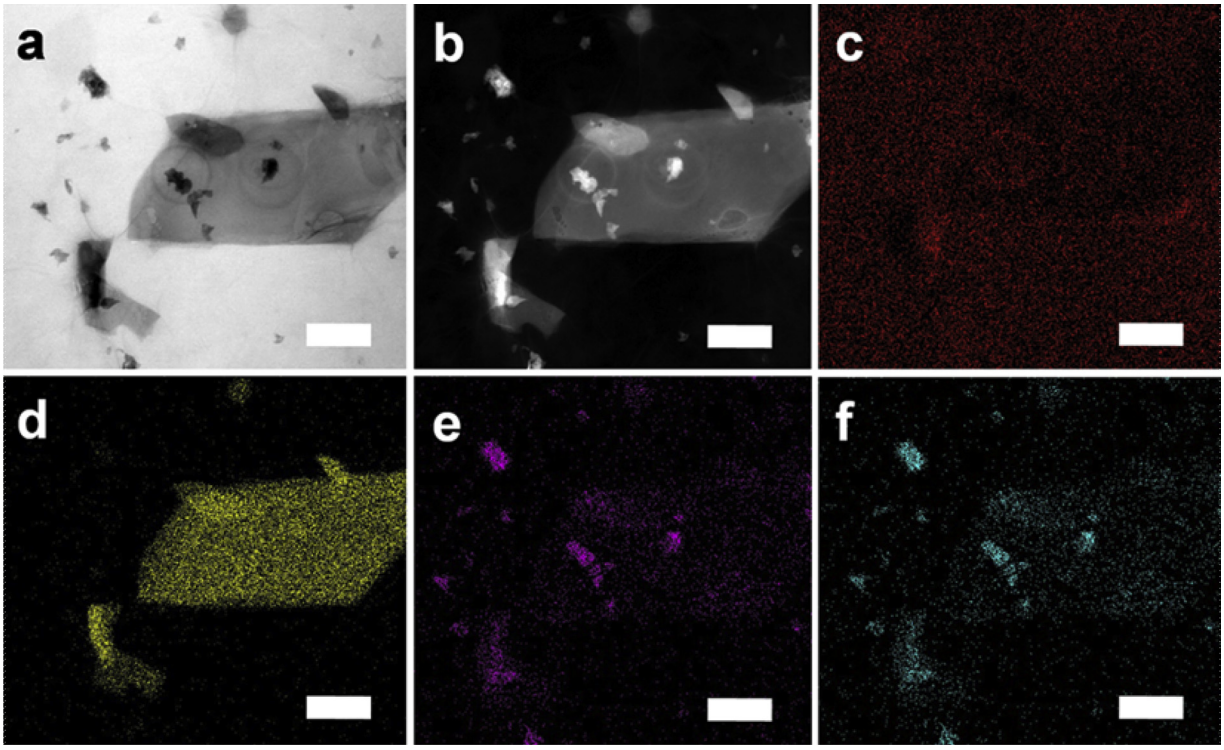

Fig. 3. TEM (a) and HAADF-STEM images (b) of MoS_2-BP/GO and corresponding EDS elemental mapping of C (c), P (d), Mo (e), and S (f) elements. The scale bars are 500 nm in the images.

exfoliation in the NMP solvent, and the size is in the range of 50 ~ 200 nm as observed in the TEM image (Fig. S4). After hybridization with BP/GO, small MoS_2 nanosheets were well dispersed on the surface of BP/GO as shown in Fig. 1b. To confirm the components of MoS_2-BP/GO, HAADF-STEM image, EDS elemental mappings and spectrum together with HRTEM image were measured. Fig. 3 clearly shows that all elements of C, P, Mo, and S were distinctly observed in MoS_2-BP/GO. Moreover, these elements were also detected in the EDS spectrum as shown in Fig. S5. To show the crystallinity of each component in MoS_2-BP/GO, HRTEM image of the as-prepared samples were analyzed. Fig. S6 shows lattice fringes with d-spacing of 0.22 and 0.62 nm, which are assigned to (002) plane of BP and MoS_2 [36], respectively. The above results solidly demonstrate the sheets on the BP/GO surface are MoS_2 nanosheets.

The chemical components of MoS_2-BP/GO were analyzed by X-ray photoelectron spectroscopy (XPS) as shown in Fig. S7. In the beginning, three characteristic peaks at 129.7, 130.6, and 133.4 eV were observed to be assigned to P $2p_{3/2}$, P $2p_{1/2}$, and oxidized phosphorus (P_xO_y), respectively [22]. Moreover, C 1s peak was deconvoluted into four bands located at 284.6, 286.6, 287.5, and 288.2 eV to be assigned to sp^2 carbon (C═C−C bonds), carbons (C−O, C═O, and O− C═O bonds), respectively, which are consistent with other reported results of GO [37]. Thirdly, two characteristic peaks are detected at 229.4 and 232.6, and 162.2 and 163.4 eV to be assigned to Mo $3d_{5/2}$ and Mo $3d_{3/2}$, and S $2p_{3/2}$ and S $2p_{1/2}$, respectively, [36] indicating the successful hybridization of MoS_2 and BP/GO.

UV–vis-NIR spectrum of the as-prepared MoS_2-BP/GO was measured as shown in Fig. 4. Firstly, BP/GO displays a broad absorption from UV to NIR region to be consistent with our previous report [21,22]. For pure MoS_2 nanosheets, the main absorption is observed in the visible region. After MoS_2 nanosheets are hybridized with BP/GO, the spectral shape of MoS_2-BP/GO is close to the overlap of MoS_2 and BP/GO, suggesting that MoS_2-BP/GO has potential photocatalytic ability under visible-NIR light irradiation.

Next, photocatalytic water reduction to H_2 is carried out to evaluate

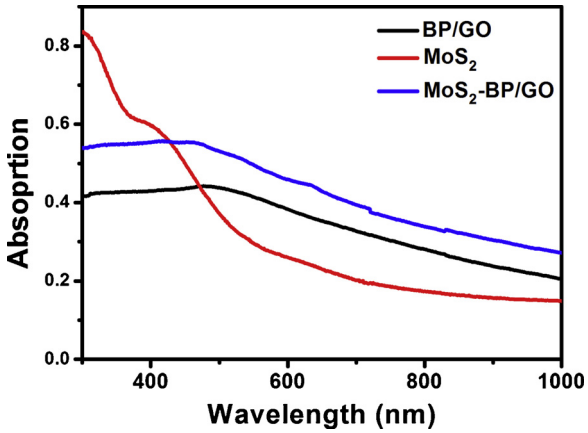

Fig. 4. UV–vis absorption spectra of as-prepared BP/GO, MoS_2, and MoS_2-BP/GO.

the photocatalytic ability of MoS_2-BP/GO because H_2 is forecast to be the most promising source of energy. To obtain the light wavelength in the visible-NIR region, a 420-nm long-pass filter was put between the reactor and the Xenon lamp (output wavelength: 350~1800 nm). As shown in Fig. 5a, pure BP and MoS_2 nanosheets did not show substantial H_2 production after visible-NIR light irradiation for 3 h, while trace H_2 (0.78 μmol) was detected with BP/GO under the same conditions. The fast recombination of photoinduced charge carriers in pure BP and MoS_2 result in no activities in BP and MoS_2, while the photogenerated electrons came from excited BP can be transferred to GO, contributing the detected H_2 in BP/GO. We also investigated the photocatalytic activity on MoS_2-BP (the corresponding TEM and EDS elemental mapping image is shown in Fig. S8). After introduction of MoS_2 as the co-catalyst, 4.58 μmol H_2 was detected after visible-NIR light irradiation for 3 h, indicating that MoS_2 nanosheets act as the efficient cocatalyst for H_2 production. When MoS_2-BP/GO was used as the

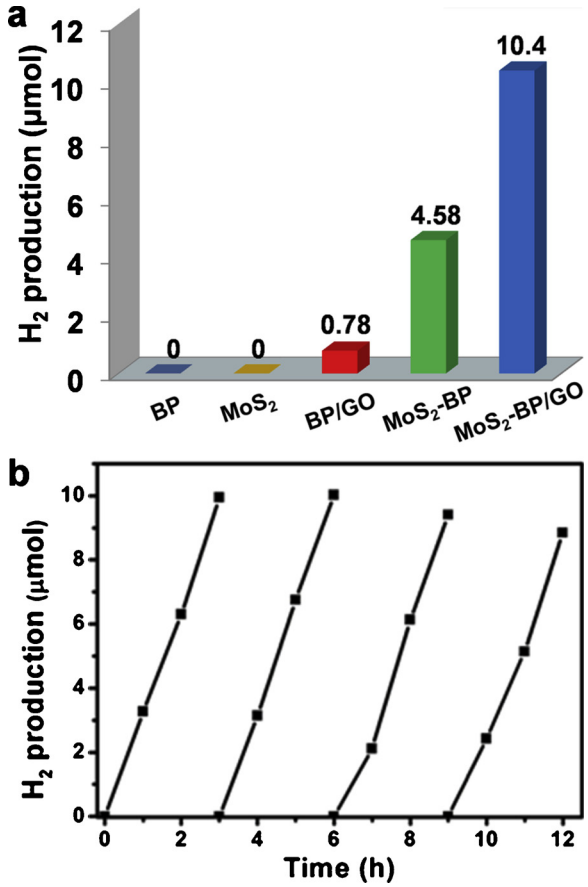

Fig. 5. Photocatalytic H_2 production with different catalysts under visible-NIR light irradiation for 3 h (a). Four cycles of photocatalytic H_2 production by using MoS_2-BP/GO (b).

photocatalyst, substantial H_2 (10.4 μmol) was detected under visible-NIR light irradiation for 3 h. Compared to BP/GO and MoS_2-BP, 13.3 and 2.27-folds enhancement in photocatalytic activity were achieved in MoS_2-BP/GO. The optimum apparent quantum efficiency (AQE) of MoS_2-BP/GO is approximately 10.1% at 420 ± 5 nm. Moreover, the control experiments of different sacrificial reagents and Pt-BP/RGO were investigated, which were shown in Fig. S9. The results show that the sample of MoS_2-BP/GO displayed simlar photocatalytic H_2 production activiy with different sacrificial reagents and Pt-BP/RGO as comparison photocatalyst.

Cyclic photocatalytic H_2 evolution experiments were carried out to investigate the durability of MoS_2-BP/GO. After the first run, the reaction mixture was bubbled with Ar and then used for subsequent runs. Fig. 5b shows continuous H_2 production with slight decrease in the subsequent four runs. This slight decrease is because: (i) the loss of catalysts during collected process for next cycle run; (ii) the degradation of BP during long time light irradiation in the aquesous solution; (iii) the decrease of the concentration of sacrificial electron donor after long time photoreaction. Moreover, TEM image and XPS spectra of MoS_2-BP/GO after photocatalytic reaction display no obvious change (Figs. S10 and S11), suggesting that MoS_2-/BP/GO keeps stable during photocatalytic H_2 production.

These results clearly show that the as-prepared ternary composite of MoS_2-BP/GO has the highest photocatalytic activity. Generally, an effective charge separation in the composite contributes to the enhancement of photocatalytic performance. Accordingly, photocurrent responses were firstly studied to clarify the interfacial charge transport in MoS_2-BP/GO. As shown in Fig. 6, when BP, BP/GO, MoS_2-BP, and MoS_2-BP/GO modified electrodes acted as the working electrodes,

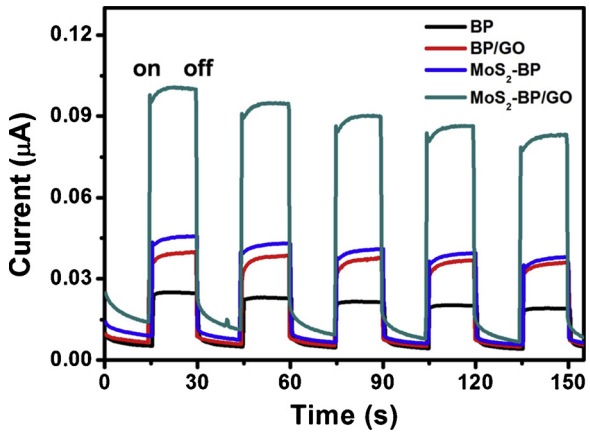

Fig. 6. Photocurrent responses of BP, BP/GO, MoS_2-BP, and MoS_2-BP/GO with on/off of the visible-NIR light irradiation.

response photocurrents with repeatable light on/off cycles were observed. The average photocurrent for MoS_2-BP/GO is approximately 0.080 μA, which is 2.4, 2.6, and 5.3 times larger than those of pure MoS_2-BP (0.033 μA), BP/GO (0.031 μA), and BP (0.015 μA), respectively, suggesting that the as-prepared MoS_2-BP/GO displays effective visible-NIR photo-response activities and MoS_2-BP/GO has the highest charge separation efficiency compared to pure BP, BP/GO, and MoS_2-BP.

Although the above photoelectrochemical properties indicate efficient charge separation in MoS_2-BP/GO, the dynamic of electron transfer is direct proof for the photocatalytic process. Transient absorption spectroscopy (TAS) is a powerful tool to analyze the dynamic of photoexcited state [38–40]. Accordingly, the TAS experiments of BP, BP/GO, and MoS_2-BP/GO were performed under 400-nm laser excitation. As shown in Fig. 7a, a broad transient absorption peak at 620 nm appeared for pure BP in the visible wavelength region (480~720 nm), indicating that BP can be excited to give electron-hole pairs under light irradiation. For BP/GO and MoS_2-BP/GO, the broad transient absorption spectra were observed as shown in Figs. 7**b** and **7c**. In the wavelength region of 660~720 nm, a weak tail absorption was appeared in both BP/GO and MoS_2-BP/GO, with comparison to that for pure BP, due to the interaction of BP with GO, and BP with MoS_2. The concentration of charges (transient absorption intensity at 620 nm) for all samples decreased via the charge recombination in a multi-exponential fashion at a time period of 0–700 ps. Moreover, at 300 ps after the excitation, the concentration of charges for pure BP decreased to 32.5% of the initial value while BP/GO and MoS_2-BP/GO decreased to 15.5% and 8.8%, respectively. The faster decrease of the concentration of charges in BP/GO and MoS_2-BP/GO indicates that electron decay process is accelerated in BP/GO and MoS_2-BP/GO compared with that in pure BP.

To evaluate the detail electron decay kinetics, the time profiles of transient absorption were fitted using two-exponential functions according to $\Delta A = \Delta A0 + \sum_i A_i e^{(-\tau/\tau_i)}$ in which A and τ_i refer to the amplitudes and lifetimes of i_{th} components, respectively. The parameters are shown in Fig. 7d and summarized in Table 1. From Table 1, it can be seen that two components with a short and a long lifetimes are observed in all samples. Generally, the shorter lifetime (τ_1) is assigned to the recombination of surface-related charge and the longer lifetime is attributed to the recombination of free excitons in semiconductors [41]. Firstly, compared with that in pure BP (τ_1 = 29.0 ps, 16.3%), in BP/GO (τ_1 = 11.1 ps, 23.2%) and MoS_2-BP/GO (τ_1 = 9.94 ps, 28.3%), τ_1 decreases gradually and the ratio of τ_1 increases gradually, suggesting that an effective electron transfer process occurs from BP to GO in BP/GO and MoS_2-BP/GO.

Secondly, the average lifetime (τ_{av}), calculated from $\tau_{av} = \sum_{i=1}^{i=n} A_i\tau_i^2 / \sum_{i=1}^{i=n} A_i\tau^i$, is used to evaluate the charge carriers separation efficiency in semiconductor photocatalyst systems [42]. As

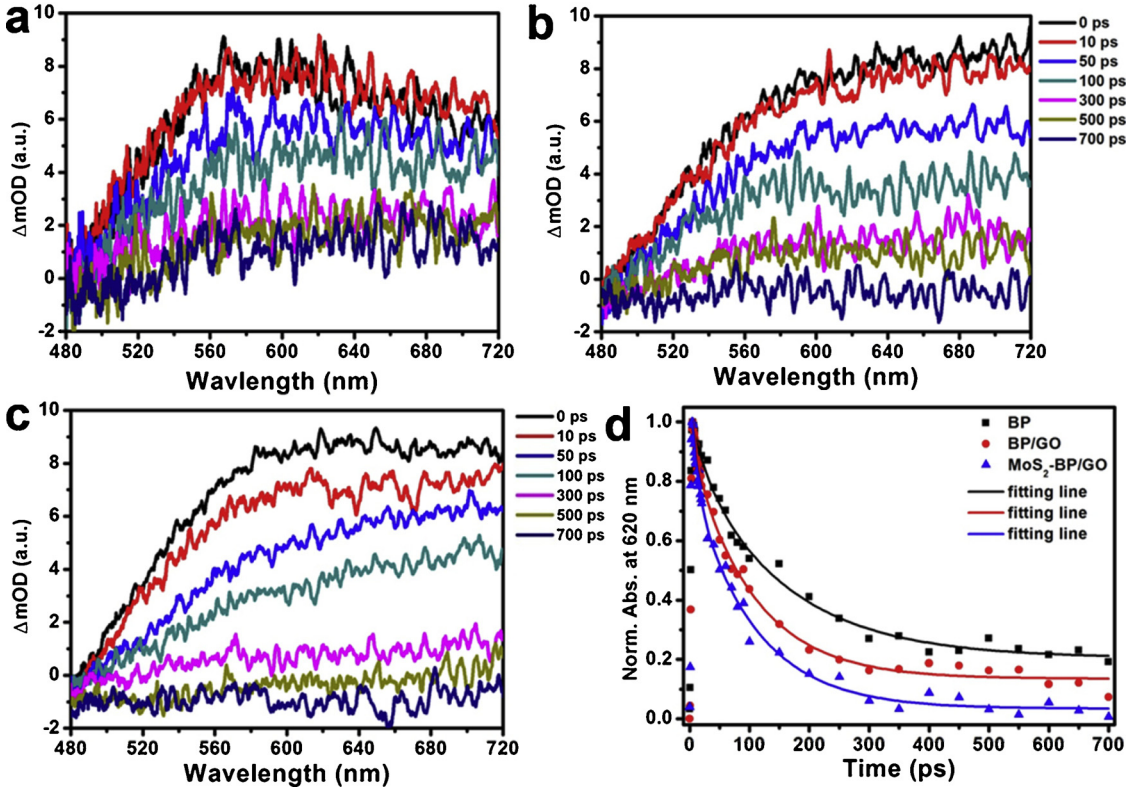

Fig. 7. Transient absorption spectra of BP (a), BP/GO (b), and MoS_2-BP/GO (c) under 400-nm laser excitation. Decay profiles of normalized transient absorption observed at 620 nm for three samples as well as the fitting lines (d).

shown in Table 1, τ_{av} of pure BP, BP/GO, and MoS_2-BP/GO are 135, 82.1, and 69.8 ps, respectively. Such decreases of τ_{av} observed with BP/GO and MoS_2-BP/GO are understood as arising from the opening of an additional channel of interfacial electron transfer from excited BP to GO, and BP to MoS_2 [42]. Similar results have been reported in other composites [43,44]. For example, Furube et al. found that τ of TiO_2 decreases after decorated with Pt nanoparticles, illustrating electrons migration from photoexcited TiO_2 to decorated Pt nanoparticles [44]. Furthermore, based on the formula of electron transfer rate (k_{ET}) and of electron injection efficiency (η_{inj}) [42,45], the k_{ET} and η_{inj} of BP/GO and MoS_2-BP/GO are estimated to be $4.77 \times 109\ s^{-1}$ and 39.2%, and $6.92 \times 10^9\ s^{-1}$ and 48.3%, respectively, indicating a fast electron transfer process occurred between excited BP and GO or MoS_2. On the other hand, k_{ET} and η_{inj} of MoS_2-BP/GO are larger than those of BP/GO, suggesting that the electron transfer occurs from excited BP not only to GO but also to the adjacent MoS_2. This result provides a straightforward evidence for the efficient transportation of photogenerated electrons between excited BP and decorated MoS_2 and GO, leading highly efficient photocatalytic H_2 production in MoS_2-BP/GO.

Based on above results, the possible mechanism for photocatalytic H_2 evolution by MoS_2-BP/GO under visible-NIR irradiation is illustrated in Fig. 8. Firstly, based on previous data [23,46], the as-prepared BP can be excited under visible-NIR light irradiation to generate electrons and holes in the CB and VB of BP, respectively. Secondly, GO works as a functional support, not only as a glue reagent for hybridization of MoS_2 as the co-catalyst on the surface of BP, but also as the catalyst's promoter to cause efficient electron transport. The CB electrons of BP can be rapidly injected to the surface of GO and then to the decorated MoS_2 nanosheets owing to the lower work function of MoS_2 [46,47]. Moreover, owing to the direct contact between BP and MoS_2, a part of electrons from excited BP is injected to MoS_2 directly. After these electrons are trapped by MoS_2, the reduction of H^+ (water) occurs to generate H_2. Finally, holes in the VB of BP are captured by methanol, which is used as a sacrificial electron donor. Accordingly, the enhanced photocatalytic activity is due to the cooperative effects of GO and MoS_2 sheets, leading an efficient charge separation/transfer.

4. Conclusions

In summary, a new noble-metal-free photocatalyst of MoS_2-BP/GO

Table 1
Kinetic parameters of transient absorption decays of BP, BP/GO, and MoS_2-BP/GO under 400-nm excitation based on the time profiles of transient absorption observed at 620 nm.

Samples	τ_1 (ps)	A_1	τ_2 (ps)	A_2	τ_{av} (ps)[a]	k_{ET} (s^{-1})[b]	η_{inj} (%)[c]
BP	29.0 (16.3%)	0.131	155 (83.7%)	0.670	135		
BP/GO	11.1 (23.2%)	0.240	104 (76.8%)	0.795	82.1	4.77×10^9	39.2%
MoS_2-BP/GO	9.94 (28.3%)	0.307	93.4 (71.7%)	0.777	69.8	6.92×10^9	48.3%

[a] The two-exponential decay curves were fitted using a non-linear least-squares method with a two-component decay law. The average lifetime (τ_{av}) was then determined using the equation: $\tau = \sum_{i=1}^{i=n} A_i\tau_i^2 / \sum_{i=1}^{i=n} A_i\tau^i$.

[b] $k_{ET} = \frac{1}{\tau_{BP/GO}} - \frac{1}{\tau_{BP}}$ or $\frac{1}{\tau_{MoS_2-BP/GO}} - \frac{1}{\tau_{BP}}$.

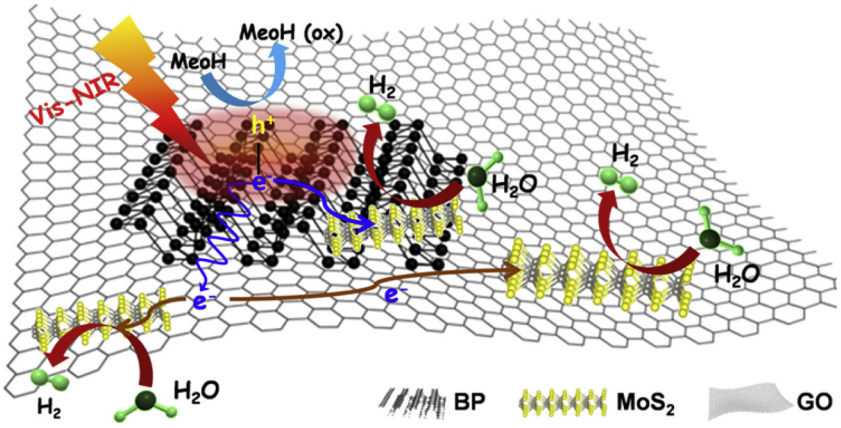

Fig. 8. Schematic illustration of MoS_2-BP/GO for photocatalytic H_2 production under visible-NIR light irradiation.

with broad wavelength absorption was constructed for the application of photocatalytic reduction of water to H_2. Herein GO shows dual functions in both synthetic process and photocatalytic H_2 production. Firstly, in the synthetic process, GO acts as a surfactant and catalyst carrier to assist the exfoliation of bulk BP and decorate MoS_2 as the co-catalyst. Secondly, GO acts as electron shuttle for promoting an efficient charge separation/transfer during photocatalytic reaction, finally contributing to the enhanced photocatalytic H_2 production. This study provides new insight into the design of broadband photocatalyst for water splitting to H_2 production and we believe that these advances make more opportunities to develop advanced function materials for artificial photosynthesis and renewable energy conversion.

Declaration of Competing Interest

The authors declare no competing financial interests.

Acknowledgments

This work has been partly supported by Grant-in-Aid for Scientific Research (project 25220806 and others) from the Ministry of Education, Culture, Sports, Science and Technology of the Japanese Government. M.Z. thanks the National Natural Science Foundation of China (21603111).

Appendix A. Supplementary data

Supplementary material related to this article can be found, in the online version, at doi:https://doi.org/10.1016/j.apcatb.2019.117864.

References

[1] H. Zhang, Ultrathin two-dimensional nanomaterials, ACS Nano 9 (2015) 9451–9469.
[2] A. Gupta, T. Sakthivel, S. Seal, Recent development in 2D materials beyond graphene, Prog. Mater. Sci. 73 (2015) 44–126.
[3] G.R. Bhimanapati, Z. Lin, V. Meunier, Y. Jung, J. Cha, S. Das, D. Xiao, Y. Son, M.S. Strano, V.R. Cooper, L. Liang, S.G. Louie, E. Ringe, W. Zhou, S.S. Kim, R.R. Naik, B.G. Sumpter, H. Terrones, F. Xia, Y. Wang, J. Zhu, D. Akinwande, N. Alem, J.A. Schuller, R.E. Schaak, M. Terrones, J.A. Robinson, Recent advances in two-dimensional materials beyond graphene, ACS Nano 9 (2015) 11509–11539.
[4] X. Kong, Q. Liu, C. Zhang, Z. Peng, Q. Chen, Elemental two-dimensional nanosheets beyond graphene, Chem. Soc. Rev. 46 (2017) 2127–2157.
[5] H. Liu, Y. Du, Y. Deng, P. Ye, Semiconducting black phosphorus: synthesis, transport properties and electronic applications, Chem. Soc. Rev. 44 (2015) 2732–2743.
[6] R. Gusmão, Z. Sofer, M. Pumera, Black phosphorus rediscovered: from bulk material to monolayers, Angew. Chem. Int. Ed. 56 (2017) 8052–8072.
[7] R. Feng, W. Lei, G. Liu, M. Liu, Visible- and nir-light responsive black-phosphorus-based nanostructures in solar fuel production and environmental remediation, Adv. Mater. 30 (2018) 1804770.
[8] H. Liu, K. Hu, D. Yan, R. Chen, Y. Zou, H. Liu, S. Wang, Recent advances on black phosphorus for energy storage, catalysis, and sensor applications, Adv. Mater. 30 (2018) 1800295.
[9] M. Rahman, C. Kwong, K. Davey, S. Qiao, 2D phosphorene as a water splitting photocatalyst: fundamentals to applications, Energy Environ. Sci. 9 (2016) 709–728.
[10] L. Li, Y. Yu, G. Ye, Q. Ge, X. Ou, H. Wu, D. Feng, X. Chen, Y. Zhang, Black phosphorus field-effect transistors, Nat. Nanotechnol. 9 (2014) 372–377.
[11] H. Wang, X. Yang, W. Shao, S. Chen, J. Xie, X. Zhang, J. Wang, Y. Xie, Ultrathin black phosphorus nanosheets for efficient singlet oxygen generation, J. Am. Chem. Soc. 137 (2015) 11376–11382.
[12] X. Zhu, T. Zhang, Z. Sun, H. Chen, J. Guan, X. Chen, H. Ji, P. Du, S. Yang, Black phosphorus revisited: a missing metal-free elemental photocatalyst for visible light hydrogen evolution, Adv. Mater. 29 (2017) 1605776.
[13] L. Bai, X. Wang, S. Tang, Y. Kang, J. Wang, Y. Yu, Z. Zhou, C. Ma, X. Zhang, J. Jiang, P.K. Chu, X. Yu, Black phosphorus/platinum heterostructure: a highly efficient photocatalyst for solar-driven chemical reactions, Adv. Mater. 30 (2018) 1803641.
[14] Y. Yuan, P. Wang, Z. Li, Y. Wu, W. Bai, Y. Su, J. Guan, S. Wu, J. Zhong, Z. Yu, Z. Zou, The role of bandgap and interface in enhancing photocatalytic H_2 generation activity of 2D-2D black phosphorus/MoS_2 photocatalyst, Appl. Catal. B 242 (2019) 1–8.
[15] L. Kong, Y. Ji, Z. Dang, J. Yan, P. Li, Y. Li, S. Liu, g-C_3N_4 loading black phosphorus quantum dot for efficient and stable photocatalytic H_2 generation under visible light, Adv. Funct. Mater. 28 (2018) 1800668.
[16] J. Hu, D. Chen, Z. Mo, N. Li, Q. Xu, H. Li, J. He, H. Xu, J. Lu, Z-scheme 2D/2D heterojunction of black phosphorus/monolayer Bi_2WO_6 nanosheets with enhanced photocatalytic activities, Angew. Chem. Int. Ed. 58 (2019) 2073–2077.
[17] B. Tian, B. Tian, B. Smith, M.C. Scott, Q. Lei, R. Hua, Y. Tian, Y. Liu, Facile bottom-up synthesis of partially oxidized black phosphorus nanosheets as metal-free photocatalyst for hydrogen evolution, Proc. Natl. Acad. Sci. U. S. A. 115 (2018) 4345–4350.
[18] L. Mao, X. Cai, S. Yang, K. Han, J. Zhang, Black phosphorus-CdS-$La_2Ti_2O_7$ ternary composite: effective noble metal-free photocatalyst for full solar spectrum activated H_2 production, Appl. Catal. B 242 (2019) 441–448.
[19] Y. Zheng, Z. Yu, H. Ou, A. Asiri, Y. Chen, X. Wang, Black phosphorus and polymeric carbon nitride heterostructure for photoinduced molecular oxygen activation, Adv. Funct. Mater. 28 (2018) 1705407.
[20] M. Zhu, X. Cai, M. Fujitsuka, J. Zhang, T. Majima, Au/$La_2Ti_2O_7$ nanostructures sensitized with black phosphorus for plasmon-enhanced photocatalytic hydrogen production in visible and near-infrared light, Angew. Chem. Int. Ed. 56 (2017) 2064–2068.
[21] M. Zhu, Y. Osakada, S. Kim, M. Fujitsuka, T. Majima, Black phosphorus: a promising two dimensional visible and near-infrared-activated photocatalyst for hydrogen evolution, Appl. Catal. B 217 (2017) 285–292.
[22] M. Zhu, S. Kim, L. Mao, M. Fujitsuka, J. Zhang, X. Wang, T. Majima, Metal-free photocatalyst for H_2 evolution in visible to near-infrared region: black phosphorus/graphitic carbon nitride, J. Am. Chem. Soc. 139 (2017) 13234–13242.
[23] M. Zhu, C. Zhai, M. Fujitsuka, T. Majima, Noble metal-free near-infrared-driven photocatalyst for hydrogen production based on 2D hybrid of black phosphorus/WS_2, Appl. Catal. B 221 (2018) 645–651.
[24] M. Zhu, Z. Sun, M. Fujitsuka, T. Majima, Z-Scheme photocatalytic water splitting on a 2D heterostructure of black phosphorus/bismuth vanadate using visible light, Angew. Chem. Int. Ed. 57 (2018) 2160–2164.
[25] J. Yan, P. Verma, Y. Kuwahara, K. Mori, H. Yamashita, Recent progress on black phosphorus-based materials for photocatalytic water splitting, Small Method 2 (2018) 1800212.
[26] J. Ran, B. Zhu, S.-Z. Qiao, Phosphorene co-catalyst advancing highly efficient visible-light photocatalytic hydrogen production, Angew. Chem. Int. Ed. 56 (2017) 10373–10377.
[27] O. Elbanna, M. Zhu, M. Fujitsuka, T. Majima, Black phosphorus sensitized TiO_2 mesocrystal photocatalyst for hydrogen evolution with visible and near-infrared light irradiation, ACS Catal. 9 (2019) 3618 − 362.
[28] J. Yan, Y. Ji, L. Kong, Y. Li, M. Navlani-García, S.F. Liu, Y. Kuwahara, K. Mori, M. Che, H. Yamashita, Black phosphorus-based compound with few layers for

photocatalytic water oxidation, ChemCatChem 10 (2018) 3424–3428.
[29] S. Lin, Y. Chui, Y. Li, S. Lau, Liquid-phase exfoliation of black phosphorus and its applications, FlatChem 2 (2017) 15–37.
[30] T. Wang, G. Zhao, C. Sun, L. Zhang, Y. Wu, X. Hao, Y. Shao, Graphene-assisted exfoliation of molybdenum disulfide to fabricate 2D heterostructure for enhancing lithium storage, Adv. Mater. Interfaces 4 (2017) 1601187.
[31] S. Deng, C.T. Cherian, X. Liu, H. Tan, L. Yeo, X. Yu, A. Rusydi, B.V.R. Chowdari, H. Fan, C. Sow, Ultrathin hexagonal hybrid nanosheets synthesized by graphene oxide-assisted exfoliation of β-$Co(OH)_2$ mesocrystals, Chem. Eur. J. 20 (2014) 12444–12452.
[32] T.T. Tung, J. Yoo, F.K. Alotaibi, M.J. Nine, R. Karunagaran, M. Krebsz, G.T. Nguyen, D.N.H. Tran, J. Feller, D. Losic, Graphene oxide-assisted liquid phase exfoliation of graphite into graphene for highly conductive film and electromechanical sensors, ACS Appl. Mater. Interfaces 8 (2016) 16521–16532.
[33] J. Kim, L.J. Cote, F. Kim, W. Yuan, K.R. Shull, J. Huang, Graphene oxide sheets at interfaces, J. Am. Chem. Soc. 132 (2010) 8180–8186.
[34] M. Zhu, P. Chen, M. Liu, High-performance visible-light-driven plasmonic photocatalysts Ag/AgCl with controlled size and shape using graphene oxide as capping agent and catalyst promoter, Langmuir 29 (2013) 9259–9268.
[35] K. Chang, X. Hai, J. Ye, Transition metal disulfides as noble-metal-alternative co-catalysts for solar hydrogen production, Adv. Energy Mater. 6 (2016) 1502555.
[36] C. Zhai, M. Sun, M. Zhu, K. Zhang, Y. Du, Insights into photo-activated electrode for boosting electrocatalytic methanol oxidation based on ultrathin MoS_2 nanosheets enwrapped CdS nanowires, Int. J. Hydrogen Energy 42 (2017) 5006–5015.
[37] M. Zhu, Z. Li, B. Xiao, Y. Lu, Y. Du, P. Yang, X. Wang, Surfactant assistance in improvement of photocatalytic hydrogen production with the porphyrin non-covalently functionalized graphene nanocomposite, ACS Appl. Mater. Interfaces 5 (2013) 1732–1740.
[38] C. Ruckebusch, M. Sliwa, P. Pernot, A. Juan, R. Tauler, Comprehensive data analysis of femtosecond transient absorption spectra: a review, J. Photochem. Photobiol. C Photochem. Rev. 13 (2012) 1–27.
[39] C. Burda, M.A. El-Sayed, High-density femtosecond transient absorption spectroscopy of semiconductor nanoparticles. A tool to investigate surface quality, Pure Appl. Chem. 72 (2000) 165–177.
[40] I. Robel, V. Subramanian, M. Kuno, P.V. Kamat, Quantum dot solar cells. Harvesting light energy with CdSe nanocrystals molecularly linked to mesoscopic TiO_2 films, J. Am. Chem. Soc. 128 (2006) 2385–2393.
[41] X. Shi, M. Fujitsuka, S. Kim, T. Majima, Faster electron injection and more active sites for efficient photocatalytic H_2 evolution in g-C_3N_4/MoS_2 hybrid, Small 14 (2018) 1703277.
[42] X. Li, W. Bi, L. Zhang, S. Tao, W. Chu, Q. Zhang, Y. Luo, C. Wu, Y. Xie, Single-atom Pt as co-catalyst for enhanced photocatalytic H_2 evolution, Adv. Mater. 28 (2016) 2427–2431.
[43] P. Yu, X. Wen, Y. Lee, W. Lee, C. Kang, J. Tang, Photoinduced ultrafast charge separation in plexcitonic CdSe/Au and CdSe/Pt nanorods, J. Phys. Chem. Lett. 4 (2013) 3596–3601.
[44] A. Furube, T. Asahi, H. Masuhara, H. Yamashita, M. Anpo, Direct observation of a picosecond charge separation process in photoexcited platinum-loaded TiO_2 particles by femtosecond diffuse reflectance spectroscopy, Chem. Phys. Lett. 336 (2001) 424–430.
[45] M. Abdellah, K. Žídek, K. Zheng, P. Chábera, M.E. Messing, T. Pullerits, Balancing electron transfer and surface passivation in gradient CdSe/ZnS core-shell quantum dots attached to ZnO, J. Phys. Chem. Lett. 4 (2013) 1760–1765.
[46] R. Feng, W. Lei, X. Sui, X. Liu, X. Qi, K. Tang, G. Liu, M. Liu, Anchoring black phosphorus quantum dots on molybdenum disulfide nanosheets: a 0D/2D nanohybrid with enhanced visible – and NIR-light photoactivity, Appl. Catal. B 238 (2018) 444–453.
[47] S. Choi, S. Zhang, W. Yang, Layer-number-dependent work function of MoS_2 nanoflakes, J. Korean Phys. Soc. 64 (2014) 1550–1555.